DOI: 10.1021/cg1007457

CRYSTAL GROWTH & DESIGN Article

2010, Vol. 10
4491–4493

Growth of Topological Insulator Bi_2Te_3 Ultrathin Films on Si(111) Investigated by Low-Energy Electron Microscopy

H. W. Liu,[†] H. T. Yuan,[‡,§] N. Fukui,[†] L. Zhang,[†] J. F. Jia,[∥] Y. Iwasa,[‡,§] M. W. Chen,*[,†] T. Hashizume,[†,⊥,#] T. Sakurai,[†] and Q. K. Xue*[,†,∥]

[†]*WPI-Advanced Institute for Materials Research, Tohoku University, Sendai 980-8577, Japan,* [‡]*Quantum-Phase Electronics Center, The University of Tokyo, Tokyo 113-8656, Japan,* [§]*Institute for Materials Research, Tohoku University, Sendai 980-8577, Japan,* [∥]*Department of Physics, Tsinghua University, Beijing 100084, China,* [⊥]*Advanced Research Laboratory, Hitachi, Ltd., Hatoyama, Saitama 350-0395, Japan, and* [#]*Department of Physics, Tokyo Institute of Technology, Meguro, Tokyo 152-8551, Japan*

Received June 3, 2010; Revised Manuscript Received August 28, 2010

ABSTRACT: The molecular beam epitaxy growth of topological insulator Bi_2Te_3 thin films on Si(111) substrates has been investigated *in situ* by low-energy electron microscopy. The crystal structure and surface morphology during growth were directly revealed, which enables us to identify the optimal growth conditions for single crystalline Bi_2Te_3 films. The formation of thin films is preceded by several surface structures, including a wetting layer and a Te/Bi-terminated Si(111)-1×1 reconstruction. Raman scattering spectra and AFM measurements indicate that, under Te-rich conditions, single crystalline films of Bi_2Te_3 grow along the [111] direction in a layer-by-layer mode. Transport measurements prove the insulating behavior of the films grown in this way.

Introduction

The narrow gap semiconductors Bi_2Te_3, Bi_2Se_3, and Sb_2Te_3 are traditional thermoelectric materials. The very recent discovery of gapless metallic states at their surface characterizes them as the so-called topological insulators (TIs).[1−7] The metallic states, which consist of a single Dirac cone induced by strong spin−orbit coupling, attract much attention due to their exotic physics. To date, the materials for TI investigations have mainly been prepared in the form of bulk crystals using a melt-growth or self-flux method.[5−7] The as-grown crystals are usually heavily n-doped due to the formation of defects, with a carrier concentration as high as 10^{19} cm^{-3}.[8] To remove the bulk electronic states, the crystals have to be heavily doped by Sn or Ca,[5−7] which can introduce impurity bands that greatly degrade the transport properties and thus device performances. It is thus highly desirable to grow intrinsic TIs in the form of thin films.

Recently, progress has been made to grow atomically smooth single-crystal Bi_2Q_3 (Q = Te, Se) thin films by molecular beam epitaxy (MBE)[9−11] and Si(111) has been used as a substrate for topological insulator film growth. However, despite its fundamental importance in understanding the growth mechanism and in growing high-quality thin films, the film growth dynamics and the surface composition is still unclear, in particular at the interface of the film and the substrate. In this study, we use low-energy electron microscopy (LEEM),[12] a powerful tool to reveal the growth and structure of thin films in real time, to investigate the crystallographic evolution during Bi_2Te_3 film growth, which offers important insights on the growth mechanism of the TI thin films.

Experimental Section

The experiments were carried out in an ultrahigh vacuum LEEM system (Elmitec GmbH, LEEM III) with a base pressure of ~3×10^{-10} Torr. Heavily doped Si(111) (n-type with phosphorus dopants, resistivity of 1−10 Ω cm) wafer was intentionally selected as substrate, not only as an epitaxial pattern for growth but also as a metallic background for transport measurements of insulating films. Clean (111)-7×7 surfaces were obtained by repeatedly flashing the samples at 1500 K. High purity Bi and Te (5 or 6 nines grade) were evaporated from two water-cooled quartz Knudsen-cells with a Te/Bi flux ratio of about 14 at elevated temperature.[10] The typical growth rate of the Bi_2Te_3 films was ~0.4 nm/min. In order to determine the crystallographic structure and the lattice parameters of the surface phases, microbeam low-energy electron diffraction (μ-LEED) images were acquired *in situ* during the film growth. The topography of the Bi_2Te_3 ultrathin films was characterized *ex situ* using atomic force microscopy (AFM) (Veeco Instruments Inc., CP-50-OL) in a tapping mode. The chemical stoichiometry of the films was characterized using a Ranishaw Raman microscope, and transport measurements were performed using a Physical Property Measurement System (PPMS, Quantum Design).

Results and Discussion

The crystal structure of Bi_2Te_3 is rhombohedral (space group D_{3d}^5) (Figure 1a).[13] Parts b−j of Figure 1 show a series of LEED patterns during deposition and a LEEM image of the grown film. The Bi−Te film growth can be classified into three stages. In stage I, once the Bi and Te shutters are opened, the LEED intensity of Si(111)-7×7 (Figure 1b) immediately becomes weak and completely disappears within a few seconds. Instead, a weak 5×5 structure appears at 0.30 monolayer (ML) coverage of Bi and Te (Figure 1c). With increasing coverage, the Si(111)-1×1 spot intensity becomes weaker while the 5×5 structure pattern turns out to be more intense and periodic, indicating the formation of a long-range ordering (Figure 1d). When the surface is covered by 1 ML atoms of Bi and Te, both the 1×1 and 5×5 patterns eventually disappear (Figure 1e). At this stage, the crystallographic phase related to Bi_2Te_3 cannot be found. Thus, deposited Bi and Te most likely form a wetting layer.

To determine which component mainly contributes to the wetting layer formation, we separately deposited Bi and Te on

*To whom correspondence should be addressed. E-mail: qkxue@mail.tsinghua.edu.cn or mwchen@wpi-aimr.tohoku.ac.jp.

Published on Web 09/15/2010

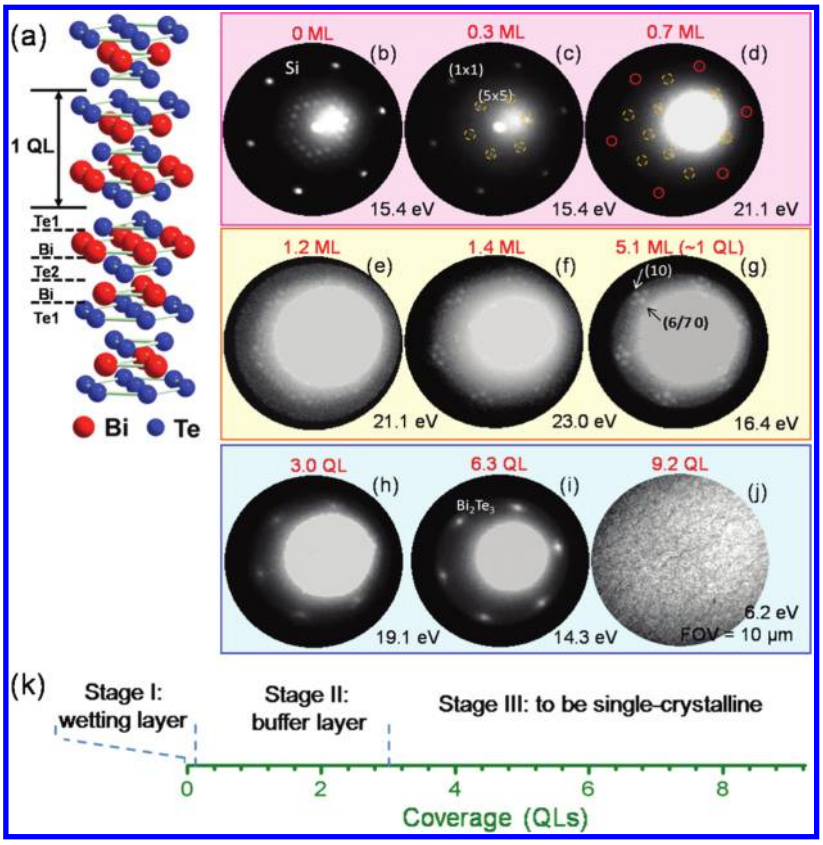

Figure 1. (a) Crystal structure of Bi_2Te_3. (b−i) Series of LEED patterns recorded *in situ* of Bi and Te deposition onto a Si(111)-7×7 surface. The Si(111)-1×1 spots are marked as red solid circles in part d, and the 5×5 structure as orange dash circles in parts c and d. (j) Bright field LEEM image of an ultrathin Bi_2Te_3 film recorded after deposition. The Bi_2Te_3 growth process with coverage is sketched in part k.

a Si(111)-7×7 surface. The 5×5 structure can be observed for Te-deposited Si(111) surfaces whereas it cannot be found on the Bi-deposited surfaces. The Te deposition time leading to the disappearance of the 7×7 and the 1×1 structures is ~25 and 14 times shorter than those of Bi. We thus suppose that although both Bi and Te contribute to the wetting layer, Te appears to play a more important role, which is consistent with previous observations on Te-terminated Si(111) surfaces.[14,15]

In stage II, a surface reconstruction can be observed on the top of the wetting layer (Figure 1e−g) when the coverage increases from 1.0 to 5.1 ML (about 1 QL). In comparison with the unit cell of the Si(111) plane (3.85 Å), the lattice constants of the reconstruction in Figure 1g are 3.88 ± 0.10 and 4.52 ± 0.11 Å for the outer and inner spots, respectively, demonstrating that those spots exactly locate at the positions (1 0) and (6/7 0) of the Si(111)-7×7 LEED pattern. Therefore, at this stage, the diffusion of coming atoms is still influenced by one unit cell because of the strong binding of exotic atoms to the DAS (dimer−adatom−stacking fault) structure, though the binding is more or less reduced by the underlying wetting layer on the Si surface. Apparently, the ultrathin film formed in this stage is a buffer layer for further Bi_2Te_3 crystal growth.

In stage III, the Bi_2Te_3 single crystal forms on the 1×1-reconstruction. As shown in Figures 1g−i, the outer spots gradually become weak while the inner spots become sharper and predominant, implying that a crystal is growing on the "distorted" 1×1-reconstruction. The lattice constant of the film is measured to be 4.36 ± 0.08 Å (Figure 1i), which is close to the value expected for the Bi_2Te_3 crystal. Since the wetting and the buffer layers reflect the periodicity and symmetry of the 7×7 lattice, the 3-fold symmetry of the Bi_2Te_3 films also agrees with that of Si(111). This result suggests that the Bi_2Te_3(111) films grow commensurately on the Si(111)-7×7 substrate with a relation of $6|a_{Bi_2Te_3}| = 7|a_{Si}|$. The lattice matching behavior of Bi_2Te_3 films on Si(111)-7×7 is similar to that of Bi grown on Si(111)-7×7.[16] Figure 1j is a bright field LEEM image of the ~9 QL Bi_2Te_3 film where terraces can be seen. Parts b−i of Figure 1 suggest a possible growth mechanism of the film that is first in the Stransky−Krastanov (S−K) mode, i.e. a three-dimensional island growth (stage II) on the initial formation of a wetting layer (stage I), and then switches from a S−K mode to a layer-by-layer (Frank−van der Merwe) mode at higher coverage (> 1 QL, stage III).[16]

The Raman spectrum (Figure 2a) of the film exhibits three characteristic peaks at 58.6, 100.2, and 139.2 cm^{-1}, which are well consistent with the A_{1g}^1, E_g^2 and A_{1g}^2 vibrational modes of Bi_2Te_3 single crystals, respectively.[17] In agreement with the Raman selection rules for a [111] film, the A_{1g} modes are enhanced when a polarizer is placed parallel to the incoming laser beam while the perpendicular configuration favors the E_g mode.[18] The topography of the Bi_2Te_3 film is characterized by AFM. As shown in Figure 2b, the film is smooth in a ~150 nm size with a root-mean-square variation of 0.4 nm. The height of the pinholes measured from the top to the underlying layer is about 1.0 nm (Figure 2c), which corresponds to the height of 1 QL of the Bi_2Te_3 crystal and confirms that our films grow with a QL-by-QL structure.

We notice that the Te/Bi flux ratio plays an important role in the Bi_2Te_3 film growth. The Bi flux directly controls the growth rate, and excess Bi makes the films more clustered and

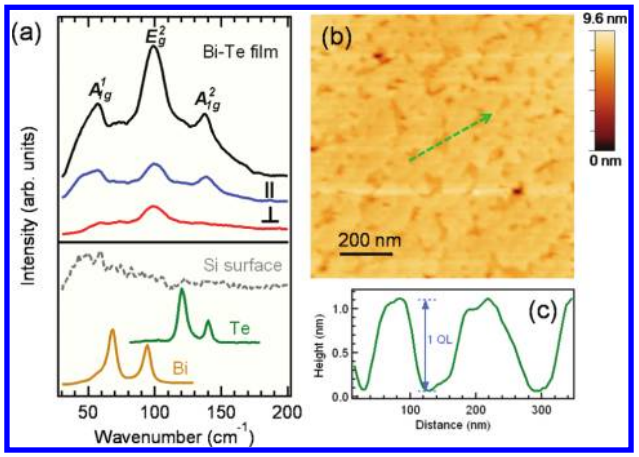

Figure 2. (a) Raman spectra of a Bi_2Te_3 film (upper frame) and Si, Bi, and Te single crystals (lower frame). The laser excitation is 632.8 nm. (b) AFM image of a Bi_2Te_3 film with a thickness of ~9 QLs. Scan size: $1 \times 1\ \mu m^2$. (c) Cross profile along the line in part b.

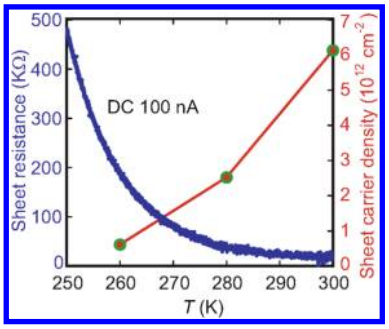

Figure 3. Temperature dependence of the resistance and carrier density of a Bi_2Te_3 ultrathin film.

not surface-flat. Bi_2Te_3 films with a good layer-by-layer structure form only at an optimal condition, which is similar to the MBE growth of GaAs under As-rich conditions.[19] From the LEED and AFM experiments, we can see that the low-coverage films, which are adsorbed on the 7×7 DAS structure, play a key role to achieve perfect wetting. The wetting layer is important to accommodate the 14% lattice mismatch between the Si(111) and Bi_2Te_3(111) planes for "coincidence lattice" formation and thereby epitaxial growth.

Figure 3 shows the temperature-dependent sheet resistance and Hall effect results on a Bi_2Te_3 ultrathin film patterning a Ti/Au Hall bar pattern. Unlike the metallic behavior in bulk crystals and cleaved flakes, the sheet resistance of ultrathin films increases drastically with temperature decreasing, indicating a semiconducting or insulting behavior. At the same time, the sheet carrier density n_s of our 5.3 nm thick film decreases from 7×10^{12} cm^{-2} at 300 K to 0.7×10^{12} cm^{-2} at 260 K when the temperature decreases. The former value corresponds to a 3D carrier density of 1.32×10^{19} cm^{-3}, which is lower than the value reported (over 3×10^{19} cm^{-3}) in non-doped bulk crystals.[21] We used the Arrhenius relation to extract an activation energy $E_{gap} = 0.48$ eV from the resistivity data that can be attributed to the band gap of the ultrathin film. This value is consistent with the value obtained from angle-resolved photoemission spectroscopy on a Bi_2Te_3 film of 1 QL thickness,[10] suggesting that the opening of the gap might be due to the quantum size effect originating from the thinness of our film. In sharp contrast with the metallic behavior of heavily doped Si substrates[21] (resistivity decreasing while cooling), such an insulating behavior of Bi_2Te_3 films indicates that the heavily doped Si substrate is not playing any role in transport measurement and the intrinsic properties of the film are probed.

Conclusions

In summary, we performed the first *in situ* LEEM investigation of the structure evolution during the Bi_2Te_3 film growth. The formation of Bi_2Te_3 single crystalline films is preceded by several surface structures, including a wetting layer and a Te/Bi-terminated Si(111)-1×1 reconstruction. Under Te-rich conditions, atomically flat (111) oriented single crystalline Bi_2Te_3 films can grow layer-by-layer on top of the wetting layer, providing high quality surfaces for studying novel quantum effects on TIs. The transport measurements support a semiconducting or insulating behavior of the films. Our work provides important information for further tailoring interface effects by utilizing various substrates.

Acknowledgment. H.W.L. is grateful to P. Richard and R. Shimizu for valuable discussions. This work is supported by the Grant-in-Aid for Young Scientists (WAKATE (B)-No. 21760022) from the Ministry of Education, Culture, Sports, Science, and Technology, also partially supported by the A3 Foresight Program from The Japan Society of Promotion of Science and National Natural Science Foundation of China.

References

(1) Bernevig, B. A.; Hughes, T. L.; Zhang, S. C. *Science* **2006**, *314*, 1757–1761.
(2) Qi, X. L.; Zhang, S. C. *Phys. Today* **2010**, *63*, 33–38.
(3) Hasan, M. Z.; Kane, C. L. **2010**, arXiv:1002.3895.
(4) Moore, J. E. *Nature* **2010**, *464*, 194–198.
(5) Xia, Y.; Qian, D.; Hsieh, D.; Wray, L.; Pal, A.; Lin, H.; Bansil, A.; Grauer, D.; Hor, Y. S.; Cava, R. J.; Hasan, M. Z. *Nat. Phys.* **2009**, *5*, 398–402.
(6) Chen, Y. L.; Analytis, J. G.; Chu, J. H.; Liu, Z. K.; Mo, S. K.; Qi, X. L.; Zhang, H. J.; Lu, D. H.; Dai, X.; Fang, Z.; Zhang, S. C.; Fisher, I. R.; Hussain, Z.; Shen, Z. X. *Science* **2009**, *325*, 178–181.
(7) Hsieh, D.; Qian, D.; Wray, L.; Xia, Y.; Hor, Y. S.; Cava, R. J.; Hasan, M. Z. *Nature* **2008**, *452*, 970–974.
(8) Urazhdin, S.; Bilc, D.; Mahanti, S. D.; Tessmer, S. H. *Phys. Rev. B* **2004**, *69*, 085313(7).
(9) Zhang, G. H.; Qin, H. J.; Teng, J.; Guo, J. D.; Guo, Q. L.; Dai, X.; Fang, Z.; Wu, K. H. *Appl. Phys. Lett.* **2009**, *95*, 053114(3).
(10) Li, Y. Y.; Wang, G.; Zhu, X. G.; Liu, M. B.; Ye, C.; Chen, X.; Wang, Y. Y.; He, K.; Wang, L. L.; Ma, X. C.; Zhang, H. J.; Dai, X.; Fang, Z.; Xie, X. C.; Liu, Y.; Qi, X. L.; Jia, J. F.; Zhang, S. C.; Xue, Q. K. *Adv. Mater.* (in press).
(11) Zhang, T.; Cheng, P.; Chen, X.; Jia, J. F.; Ma, X. C.; He, K.; Wang, L. L.; Zhang, H. J.; Dai, X.; Fang, Z.; Xie, X. C.; Xue, Q. K. *Phys. Rev. Lett.* **2009**, *103*, 266803(4).
(12) Bauer, E. *Rep. Prog. Phys.* **1994**, *57*, 895–938.
(13) Wyckoff, R. G. *Crystal Structures*; Wiley: New York, 1967; Vol. 2.
(14) Kanai, Y.; Yasue, T.; Koshikawa, T. E. *J. Surf. Sci. Nanotechnol.* **2006**, *4*, 406–409.
(15) Becker, R. S.; Golovchenko, J. A.; Swartzentruber, B. S. *Phys. Rev. B* **1985**, *32*, 8455–8457.
(16) Nagao, T.; Sadowski, J. T.; Saito, M.; Yaginuma, S.; Fujikawa, Y.; Kogure, T.; Ohno, T.; Hasegawa, Y.; Hasegawa, S.; Sakurai, T. *Phys. Rev. Lett.* **2004**, *93*, 105501(4).
(17) Kullmann, W.; Geuts, J.; Richter, W.; Lehner, N.; Rauh, H.; Steigenberger, U.; Eichhorn, G.; Geick, R. *Phys. Status Solidi B* **1984**, *125*, 131–138.
(18) Richter, W.; Kohler, H.; Becker, C. R. *Phys. Status Solidi B* **1977**, *84*, 619–628.
(19) Xue, Q. K.; Hashizume, T.; Sakurai, T. *Prog. Surf. Sci.* **1997**, *56*, 1–131.
(20) Analytis, J. G.; McDonald, R. D.; Riggs, S. C.; Chu, J.-H.; Boebinger, G. S.; Fisher, I. R. **2010**, arXiv:1003.1713v1.
(21) Li, S. S.; Thurber, W. R. *Solid-State Electron.* **1977**, *20*, 609–616.